J|A|C|S
ARTICLES
Published on Web 08/02/2002

# Probing the Electronic Structure of $[MoOS_4]^-$ Centers Using Anionic Photoelectron Spectroscopy

Xue-Bin Wang,[†] Frank E. Inscore,[‡] Xin Yang,[†] J. Jon A. Cooney,[‡] John H. Enemark,*[,‡] and Lai-Sheng Wang*[,†]

*Contribution from the Department of Physics, Washington State University, 2710 University Drive, Richland, Washington 99352, W.R. Wiley Environmental Molecular Sciences Laboratory, MS K8-88, P.O. Box 999, Pacific Northwest National Laboratory, Richland, Washington 99352, and Department of Chemistry, University of Arizona, Tucson, Arizona 85721*

Received April 16, 2002

***Abstract:*** Using photodetachment photoelectron spectroscopy (PES) in the gas phase, we investigated the electronic structure and chemical bonding of six anionic $[Mo^{V}O]^{3+}$ complexes, $[MoOX_4]^-$ (where X = Cl (**1**), SPh (**2**), and SPh-*p*-Cl (**3**)), $[MoO(edt)_2]^-$ (**4**), $[MoO(bdt)_2]^-$ (**5**), and $[MoO(bdtCl_2)_2]^-$ (**6**) (where edt = ethane-1,2-dithiolate, bdt = benzene-1,2-dithiolate, and $bdtCl_2$ = 3,6-dichlorobenzene-1,2-dithiolate). The gas-phase PES data revealed a wealth of new electronic structure information about the $[Mo^{V}O]^{3+}$ complexes. The energy separations between the highest occupied molecular orbital (HOMO) and HOMO−1 were observed to be dependent on the O−Mo−S−C(α) dihedral angles and ligand types, being relatively large for the monodentate ligands, 1.32 eV for Cl and 0.78 eV for SPh and SPhCl, compared to those of the bidentate dithiolate complexes, 0.47 eV for edt and 0.44 eV for bdt and $bdtCl_2$. The threshold PES feature in all six species is shown to have the same origin and is due to detaching the single unpaired electron in the HOMO, mainly of Mo 4d character. This result is consistent with previous theoretical calculations and is verified by comparison with the PES spectra of two $d^0$ complexes, $[VO(bdt)_2]^-$ and $[VO(bdtCl_2)_2]^-$. The observed PES features are interpreted on the basis of theoretical calculations and previous spectroscopic studies in the condensed phase.

## Introduction

Metalloenzymes that contain a single Mo or W atom at the active site are now well known.[1−3] An unusual but common feature of these enzymes is the presence of one or two pyranopterin dithiolate units, which are coordinated to the metal by the two sulfur atoms of the ene-1,2-dithiolate chelate portion of the tricyclic ring, as shown in Figure 1.[4−20] The Mo-containing enzymes are proposed to cycle through Mo(VI/V/IV) oxidation states during turnover conditions and catalyze specific two-electron redox processes that are formally coupled

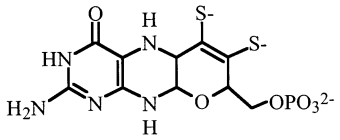

***Figure 1.*** Structure of the pyranopterin cofactor derived from protein X-ray crystallographic studies.[4−20]

* To whom correspondence should be addressed. E-mail: jenemark@u.arizona.edu and ls.wang@pnl.gov.

[†] Washington State University and Pacific Northwest National Laboratory.

[‡] University of Arizona.

(1) Hille, R. *Chem. Rev.* **1996**, *96*, 2757−2816.
(2) Johnson, M. K.; Rees, D. C.; Adams, M. W. *Chem. Rev.* **1996**, *96*, 2817−2839.
(3) *Molybdenum and Tungsten, Their Roles in Biological Processes*; Sigel, A., Sigel, H., Eds.; Metal Ions in Biological Systems 39; Dekker: New York, 2002; 759 pp.
(4) Kisker, C.; Schindelin, H.; Pacheco, A.; Wehbi, W. A.; Garrett, R. M.; Rajagopalan, K. V.; Enemark, J. H.; Rees, D. C. *Cell* **1997**, *91*, 973−983.
(5) Romão, M. J.; Archer, M.; Moura, I.; Moura, J. J. G.; LeGall, J.; Engh, R.; Schneider, M.; Hof, P.; Huber, R. *Science* **1995**, *270*, 1170−1176.
(6) Huber, R.; Hof, P.; Duarte, R. O.; Moura, J. J. G.; Moura, I.; Liu, M. Y.; LeGall, J.; Hille, R.; Archer, M.; Romão, M. J. *Proc. Natl. Acad. Sci. U.S.A.* **1996**, *93*, 8846−8851.
(7) Rebelo, J.; Macieira, S.; Dias, J. M.; Huber, R.; Ascenso, C. S.; Rusnak, F.; Moura, J. J. G.; Moura, I.; Romão, M. J. *J. Mol. Biol.* **2000**, *297*, 135−146.
(8) Schneider, F.; Löwe, J.; Huber, R.; Schindelin, H.; Kisker, C.; Knäblein, J. *J. Mol. Biol.* **1996**, *263*, 53−69.
(9) McAlpine, A. S.; McEwan, A. G.; Shaw, A. L.; Bailey, S. *J. Biol. Inorg. Chem.* **1997**, *2*, 690−701.
(10) Schindelin, H.; Kisker, C.; Hilton, J.; Rajagopalan, K. V.; Rees, D. C. *Science* **1996**, *272*, 1615−1621.
(11) Li, H. K.; Temple, C.; Rajagopalan, K. V.; Schindelin, H. *J. Am. Chem. Soc.* **2000**, *122*, 7673−7680.
(12) Boyington, J. C.; Gladyshev, V. N.; Khangulov, S. V.; Stadtman, T. C.; Sun, P. D. *Science* **1997**, *275*, 1305.
(13) Czjzek, M.; Santos, J. P.; Pommier, J.; Giordano, G.; Mejean, V.; Haser, R. *J. Mol. Biol.* **1998**, *284*, 435−447.
(14) Dias, J. M.; Than, M. E.; Humm, A.; Bourenkov, G. P.; Bartunik, H. D.; Bursakov, S.; Calvete, J.; Caldeira, J.; Carneiro, C.; Moura, J. J. G.; Romão, M. J. *Structure* **1999**, *7*, 65.
(15) Stewart, L. J.; Baily, S.; Bennett, B.; Charnock, J. M.; Garner, C. D.; McAlpine, A. S. *J. Mol. Biol.* **2000**, *299*, 593−600.
(16) McAlpine, A. S.; McEwan, A. G.; Bailey, S. *J. Mol. Biol.* **1998**, *275*, 613−623.
(17) Rebelo, J. M.; Dias, J. M.; Huber, R.; Moura, J. G.; Romão, M. J. *J. Biol. Inorg. Chem.* **2001**, *6*, 791−800.
(18) Enroth, C.; Eger, B.; Okamoto, K.; Nishino, T.; Nishino, T.; Pai, E. F. *Proc. Natl. Acad. Sci. U.S.A.* **2000**, *97*, 10723−10728.
(19) Chan, M. K.; Mukund, S.; Kletzin, A.; Adams, M. W. W.; Rees, D. C. *Science* **1995**, *267*, 1463−1469.
(20) Hu, Y.; Faham, S.; Roy, R.; Adams, M. W.; Rees, D. C. *J. Mol. Biol.* **1999**, *286*, 899−914.


**10.1021/ja0265557 CCC: $22.00** 

to oxygen atom transfer (OAT). These enzymes belong to three structurally distinct families [sulfite oxidase, xanthine oxidase, and dimethylsulfoxide (DMSO) reductase].[1] The DMSO reductase family[8−16] is unique because the Mo atom is coordinated by two pyranopterin ene-1,2-dithiolates; this contrasts to the single pyranopterin dithiolate observed for the sulfite oxidase[4] and xanthine oxidase families.[5−7,17,18] This pyranopterin dithiolate unit is postulated to act as an electron conduit (superexchange pathway) for electron-transfer (ET) regeneration of the active site[21] and may also play a role in modulating the metal redox potential.[1,21,22] The absence of additional redox centers in the DMSO reductases from *Rhodobacter sphaeroides* and *Rhodobacter capsulatus* has provided unique opportunities to probe the geometric and electronic structures of these active sites by a variety of spectroscopic techniques, including X-ray absorption, electron paramagnetic resonance (EPR), electronic absorption, magnetic circular dichroism, and resonance Raman spectroscopy.[23−35] Similar spectroscopic studies of oxidized biotin sulfoxide reductase from *R. sphaeroides* expressed in *Escherichia coli* have also been reported.[36]

The results of these structural and spectroscopic studies have provided the motivation to synthesize and characterize a variety of $\{Mo(O)S_4\}$ complexes as small inorganic molecular analogues of the DMSO reductase active sites in order to evaluate the role of the pyranopterin dithiolate S donors in catalysis. Holm and co-workers have been particularly active in this area and have provided a variety of new Mo (and W) compounds relevant to the DMSO reductase active site.[37−44] Mo compounds possessing paramagnetic $\{Mo^VOS_4\}^-$ centers are amenable to study by a variety of spectroscopic techniques [EPR, electronic absorption, magnetic circular dichroism (MCD), and resonance Raman] that are well suited for investigating S→Mo charge-transfer (CT) transitions in these centers. In conjunction with density functional theory (DFT) calculations, such detailed spectroscopic studies have provided much insight into Mo−S bonding and covalency within the $[Mo^VOS_4]^-$ systems for a variety of oxo-Mo(V) tetrathiolates[45,46] and oxo-Mo(V) bis-dithiolates.[45,47] It should be noted that DFT calculations have also been utilized and reported for studying organometallic dithiolenes[48] and other systems relating to ET[49] and OAT[50−54] in the active sites of the pyranopterin Mo and W enzymes. However, ambiguities still remain regarding the exact nature of certain spectral features and the molecular orbital description of the ground state in the series of $[MoOS_4]^-$ complexes.[45−47]

Photoelectron spectroscopy (PES) is a powerful technique for studying the electronic structure and chemical bonding of molecules. PES has been used to study numerous metal complexes,[55] including oxo-molybdenum complexes possessing an ene-1,2-dithiolate ligand.[56,57] The relevant PES studies reported so far are for neutral molecules in the gas phase, which limits the application of PES to compounds with sufficient volatility and thermal stability. We have recently developed a new experimental technique, which couples an electrospray ionization (ESI) source with a magnetic-bottle PES apparatus.[58] ESI is a versatile technique, allowing ionic species in solution samples to be transported into the gas phase. Our recent research has shown that the new ESI−PES technique is ideal for investigating multiply charged anions in the gas phase,[59] as well as anionic metal complexes commonly present in solution.[60−64] PES of such metal complexes in the gas phase allows their intrinsic electronic structures to be probed without the complication of the solvents.

Herein we report a PES study of a series of $[Mo^VOS_4]^-$ anionic complexes in the gas phase. We were interested in probing the electronic structures of the Mo complexes and addressing issues related to the nature of their redox orbitals and the chemical bonding between the Mo and ligand S atoms. This study was also aimed at providing additional insight into the electronic properties of monoanionic oxo-Mo(V) systems


(21) Inscore, F. E.; McNaughton, R.; Westcott, B. L.; Helton, M. E.; Jones, R.; Dhawan, I. K.; Enemark, J. H.; Kirk, M. L. *Inorg. Chem.* **1999**, *38*, 1401−1410.
(22) Helton, M. E.; Kirk, M. L. *Inorg. Chem*. **1999**, *38*, 4384−4385.
(23) George, G. N.; Hilton, J.; Rajagopalan, K. V. *J. Am. Chem. Soc.* **1996**, *118*, 1113−1117.
(24) George, G. N.; Hilton, J.; Temple, C.; Prince, R. C.; Rajagopalan, K. V. *J. Am. Chem. Soc.* **1999**, *121*, 1256.
(25) Adams, B.; Smith, A.; Bailey, S.; McEwan, A.; Bray, R. *Biochemistry* **1999**, *38*, 8501−8511.
(26) Bray, R.; Adams, B.; Smith, A.; Bennett, B.; Bailey, S. *Biochemistry* **2000**, *39*, 11258−11269.
(27) Bray, R.; Adams, B.; Smith, A.; Richards, R.; Lowe, D.; Bailey, S. *Biochemistry* **2001**, *40*, 9810−9820.
(28) Finnegan, M. G.; Hilton, J.; Rajagopalan, K. V.; Johnson, M. K. *Inorg. Chem.* **1993**, *32*, 2616−2617.
(29) Benson, N.; Farrar, J. A.; McEwan, A. G.; Thomson, A. J. *FEBS Lett.* **1992**, *307*, 169−172.
(30) Bastian, N. R.; Kay, C. J.; Barber, M. J.; Rajagopalan, K. V. *J. Biol. Chem.* **1991**, *266*, 45.
(31) Bennett, B.; Benson, N.; McEwan, A.; Bray, R. *Eur. J. Biochem.* **1994**, *255*, 321−331.
(32) Gruber, S.; Kilpatrick, L.; Bastian, N.; Rajagopalan, K. V.; Spiro, T. G. *J. Am. Chem. Soc.* **1990**, *112*, 8179.
(33) Kilpatrick, L.; Rajagopalan, K. V.; Hilton, J.; Bastian, N.; Steifel, E.; Pilato, R.; Spiro, T. G. *Biochemistry* **1995**, *34*, 3032−3039.
(34) Garton, S.; Hilton, J.; Oku, H.; Crouse, B.; Rajagopalan, K.; Johnson, M. K. *J. Am. Chem. Soc.* **1997**, *119*, 12906−12916.
(35) Garton, S.; Garrett, R. M.; Rajagopalan, K V.; Johnson, M. K. *J. Am. Chem. Soc.* **1997**, *119*, 2590−2591.
(36) Temple, C.; George, G.; Hilton, J.; George, M.; Prince, R.; Barber, M.; Rajagopalan, K. V. *Biochemistry* **2000**, *39*, 4046−4052.
(37) Lim, B. S.; Willer, M. W.; Miao, M.; Holm, R. H. *J. Am. Chem. Soc.* **2001**, *123*, 8343−8349.
(38) Sung, K.; Holm, R. H. *J. Am. Chem. Soc.* **2001**, *123*, 1931−1943.
(39) Lim, B. S.; Holm, R. H. *J. Am. Chem. Soc.* **2001**, *123*, 1920−1930.
(40) Musgrave, K.; Lim, B.; Sung, K.; Holm, R. H. *Inorg. Chem.* **2000**, *39*, 5238−5247.
(41) Musgrave, K.; Donahue, J.; Lorber, C.; Holm, R. H.; Hedman, B.; Hodgson, K. *J. Am. Chem. Soc.* **1999**, *121*, 10297−10307.
(42) Donahue, J.; Goldsmith, C.; Nadiminti, U.; Holm, R. H. *J. Am. Chem. Soc.* **1998**, *120*, 12869−12881.
(43) Donahue, J.; Lorber, C.; Nordlander, E.; Holm, R. H. *J. Am. Chem. Soc.* **1998**, *120*, 3259.
(44) Lim; B.; Donahue, J.; Holm, R. H. *Inorg. Chem.* **2000**, *39*, 263−273.
(45) McMaster, J.; Carducci, M.; Yang, Y.; Solomon, E. I.; Enemark, J. H. *Inorg. Chem.* **2001**, *40*, 687−702.
(46) McNaughton, R.; Tipton, A.; Rubie, N.; Conry, R.; Kirk, M. L. *Inorg. Chem.* **2000**, *39*, 5697−5706.
(47) McNaughton, R.; Helton, M. E.; Rubie, N.; Kirk, M. L. *Inorg. Chem.* **2000**, *39*, 4386-4387.
(48) Domercq, B.; Coulon, C.; Fourmigue, M. *Inorg. Chem.* **2001**, *40*, 371−378.
(49) Fomitchev, D. V.; Lim, B. S.; Holm, R. H. *Inorg. Chem.* **2001**, *40*, 645−654.
(50) Webster, C. E.; Hall, M. *J. Am. Chem. Soc.* **2001**, *123*, 5820−5821.
(51) Thomson, L. M.; Hall, M. *J. Am. Chem. Soc.* **2001**, *123*, 3995−4002.
(52) Thapper, A.; Deeth, R. J.; Nordlander, E. *Inorg. Chem.* **1999**, *38*, 1015−1018.
(53) Voityuk, A. A.; Albert, K.; Kostlmeier, S.; Nasluzov, V. A.; Neyman, K. M.; Hof, P.; Huber, R.; Romão, M. J.; Rosch, N. *J. Am. Chem. Soc.* **1997**, *119*, 3159−3160.
(54) Bray, M. R.; Deeth, R. J. *Inorg. Chem.* **1996**, *35*, 5720−5724.
(55) Chang, C. S. J.; Rai-Chaudhuri, A.; Lichtenberger, D. L.; Enemark, J. H. *Polyhedron* **1990**, *9*, 1965−1969.
(56) Westcott, B. L.; Gruhn, N. E.; Enemark, J. H. *J. Am. Chem. Soc.* **1998**, *120*, 3382−3386.
(57) Westcott, B. L.; Enemark, J. H. *Inorg. Chem.* **1997**, *36*, 5404−5405.
(58) Wang, L. S.; Ding, C. F.; Wang, X. B.; Barlow, S. E. *Rev. Sci. Instrum.* **1999**, *70*, 1957−1966.
(59) Wang, L. S.; Wang, X. B. *J. Phys. Chem. A* **2000**, *104*, 1978−1990.
(60) Wang, X. B.; Wang, L. S.; Brown, R.; Schwerdtfeger, P.; Schröder, D.; Schwarz, H. *J. Chem. Phys*. **2001**, *114*, 7388−7395.
(61) Wang, X. B.; Wang, L. S. *J. Phys. Chem. A* **2000**, *104*, 4429−4432.
(62) Wang, X. B.; Wang, L. S. *J. Chem. Phys.* **2000**, *112*, 6959−6962.
(63) Wang, X. B.; Wang, L. S. *J. Am. Chem. Soc.* **2000**, *122*, 2339−2345.
(64) Wang, X. B.; Wang, L. S. *J. Am. Chem. Soc.* **2000**, *122*, 2096−2100.

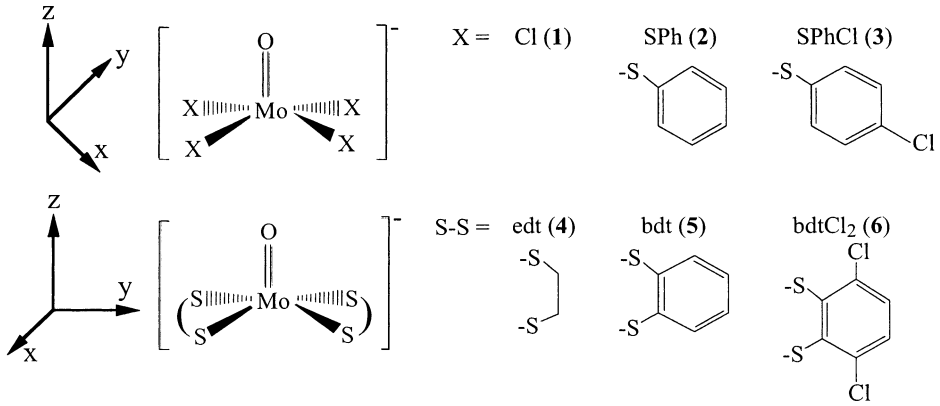


***Figure 2.*** Schematic structures of $[MoOCl_4]^-$ (**1**) and the five $[MoOS_4]^-$ compounds (**2**−**6**). The nomenclature $[MoOS_4]^-$ has been used to designate a four-sulfur center comprising the inner coordination sphere about Mo in these five-coordinate oxo-Mo(V) complexes. The thiolate $(SR)^-$ and dithiolate $(S-S)^{2-}$ ligands are shown in their respective monoanionic and dianionic forms. The coordinate systems for the oxo-Mo(V) complexes use idealized $C_{4v}$ and $C_{2v}$ structures.

that are structurally related to the active sites of the DMSO reductase family of pyranopterin Mo enzymes.

## Experimental Details

**Synthesis.** All reactions and synthetic operations, unless noted otherwise, were performed under a dry inert atmosphere of prepurified argon using Schlenk techniques, a double-line high-vacuum/gas manifold, and a polyethylene glovebag. All glassware and accessories were heated, purged with argon, and when possible evacuated prior to use. THF was dried and purified by distillation over sodium/benzophenone. All other solvents ($CCl_4$, $CH_3CN$, $CH_2Cl_2$, MeOH, $Et_2O$) were used as received (Drisolv; EM Science). These solvents were thoroughly degassed by repeated freeze−pump−thaw cycles and transferred to reaction vessels via steel cannula techniques under a positive pressure of dry argon. The reagents (Aldrich), $MoCl_5$, tetraphenyl phosphonium, and tetraphenyl arsonium chloride salts, were dried in vacuo prior to use. The ligands (Aldrich), thiophenol (HSPh), 4-chlorothiophenol (HSPhCl), 1,2-ethanedithiol ($H_2$edt), and 3,6-dichloro-1,2-benzenedithiol ($H_2$bdtCl$_2$), were distilled and/or dried in vacuo prior to use. 1,2-Benzenedithiol ($H_2$bdt) was synthesized according to literature precedent[65] and purified by vacuum distillation. The $[PPh_4]^+$ salts of $[MoOCl_4]^-$ (**1**), $[MoO(SPh)_4]^-$ (**2**), and $[MoO(SPhCl)_4]^-$ (**3**) were prepared according to published methods.[66−68]

The syntheses of the $[PPh_4]^+$ salts of $[MoO(edt)_2]^-$ (**4**) and $[MoO(bdt)_2]^-$ (**5**) were reported previously.[69,70] A modification of this procedure was used here to synthesize and purify the $[PPh_4]^+$ salt of a new complex, $[MoO(bdtCl_2)_2]^-$ (**6**). To an evacuated flask, a mixture of precursor **2** suspended in $CH_2Cl_2$ (23 °C) was added, followed by 2 equiv of the $H_2$bdtCl$_2$ proligand, which was stirred under argon for 4.5 h and then filtered anaerobically. The resulting solution was then transferred onto a coarse glass frit (filter tube) connected to a flask containing $Et_2O$. A positive pressure of argon through the flask provided a slow diffusion of $Et_2O$ vapor into the solution maintained on top of the frit. The slow stream of $Et_2O$ forced through this saturated solution eventually effected a dark black/green material to precipitate out, which was subsequently collected by filtration and washed with $Et_2O$ followed by cold MeOH to remove any unreacted dithiol. The powder collected was dissolved in a minimum amount of $CH_2Cl_2$ and layered with $Et_2O$ in a 1:4 ratio. Green-black crystals of **6** were filtered and washed with $Et_2O$.

$[HNEt_3]_2[VO(bdt)_2]$ and $[HNEt_3]_2[VO(bdtCl_2)_2]$ were prepared under argon from $VO(acac)_2$ and the respective dithiol proligand by ligand exchange in the presence of distilled, dry triethylamine, as described by Cooney et al.[71] The monoanionic V(V) species, $[VO(bdt)_2]^-$ (**7**) and $[VO(bdtCl_2)_2]^-$ (**8**), were generated from the respective dianionic V(IV) species in situ and isolated by time-of-flight (TOF) mass spectrometry as described below for PES studies. The oxo-Mo(V) complexes (Figure 2) were characterized by HR-ESI(±) in $CH_3CN$. The $(PPh_4)[MoOS_4]$ compounds investigated in this study are air sensitive, especially in solution. Hence, the preparation and manipulation of these samples required the rigorous exclusion of both oxygen and water. Samples were stored in a dry, inert atmospheric glovebox until needed.

**Photodetachment Photoelectron Spectroscopy.** Details of the ESI−PES apparatus were published elsewhere.[58] Only a brief description of the experimental procedure is given here. To produce the desired anions, we used $10^{-3}$ M solutions of the $[PPh_4]^+$ salts of **1**−**6**, respectively, in a pure and oxygen-free $CH_3CN$ solvent. The solutions were sprayed through a 0.01-mm-diameter syringe needle biased at −2.2 kV in a nitrogen atmosphere. Negatively charged ions emerging from a desolvation capillary were guided by a radio-frequency-only quadrupole ion guide into an ion trap, where the ions were accumulated for 0.1 s before being pushed into the extraction zone of a TOF mass spectrometer. The main anion signals corresponded to the anionic species of each compound. The anions of interest were mass-selected and decelerated before being intercepted by a laser beam in the detachment zone of the magnetic-bottle PES analyzer. For the current study, 266 nm (4.661 eV) photons from a Q-switched Nd:YAG laser and 193 (6.424 eV) and 157 nm (7.866 eV) photons from an excimer laser were used for photodetachment. Photoelectrons were collected at nearly 100% efficiency by the magnetic-bottle and analyzed in a 4-m-long TOF tube. Photoelectron TOF spectra were collected and then converted to kinetic energy spectra, calibrated by the known spectra of $I^-$ and $O^-$. The binding energy spectra were obtained by subtracting the kinetic energy spectra from the corresponding photon energies. The energy resolution ($\Delta E/E$) was about 2% (fwhm), i.e., ∼10 meV for 0.5 eV electrons, as measured from the spectrum of $I^-$ at 355 nm.

**Theoretical Methods.** The $[MoO(edt)_2]^-$ (**4**) and $[MoO(bdt)_2]^-$ (**5**) anions were also studied theoretically using the Amsterdam density functional (ADF version 2000.01) program package.[72−75] The geom-

(65) Giolando, D. M.; Kirschbaum, K. *Synthesis* **1992**, 451−460.
(66) Carducci, M. D.; Brown, C.; Solomon, E. I.; Enemark, J. H. *J. Am. Chem. Soc.* **1994**, *116*, 11856−11868.
(67) Boyd, I.; Dance, I.; Murray, K.; Wedd, A. *Aust. J. Chem.* **1978**, *31*, 279−284.
(68) Ellis, S.; Collison, D.; Garner, C. *J. Chem. Soc., Dalton Trans.* **1989**, 413−417.
(69) Ellis, S.; Collison, D.; Garner, C.; Clegg, W. *J. Chem. Soc., Chem. Commun.* **1986**, 1483−1485.
(70) Boyde, S.; Ellis, S.; Garner, C.; Clegg, W. *J. Chem. Soc., Chem. Commun.* **1986**, 1541−1543.
(71) Cooney, J.; Carducci, M. D.; McElhaney, A. E.; Selby, H.; Enemark, J. H., submitted for publication.
(72) Baerends, E. J.; Ellis, D. E.; Ros, P. *Chem. Phys.* **1973**, *2*, 41−51.

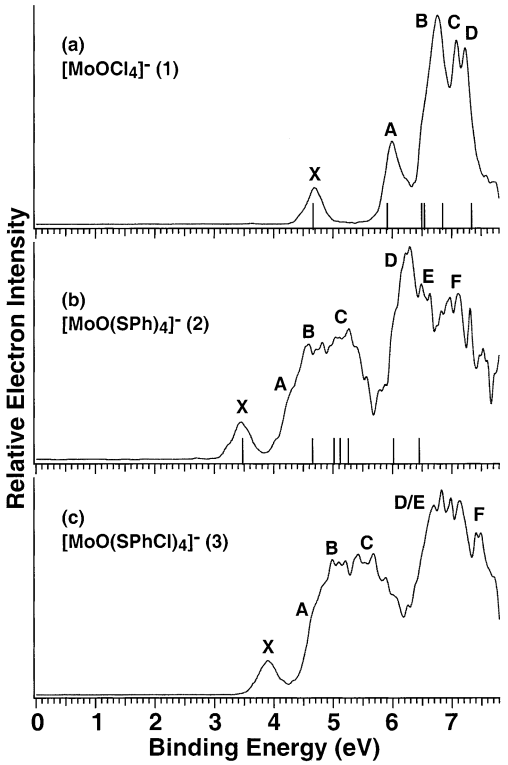


***Figure 3.*** Photoelectron spectra of (a) $[MoOCl_4]^-$ (**1**), (b) $[MoO(SPh)_4]^-$ (**2**), and (c) $[MoO(SPhCl)_4]^-$ (**3**) at 157 nm (7.866 eV). The solid bars are the molecular orbital energy levels calculated for $[MoOCl_4]^-$ and the model compound $[MoO(SCH_3)_4]^-$ using Koopmanns' approximation (see text and Tables 2 and 3).

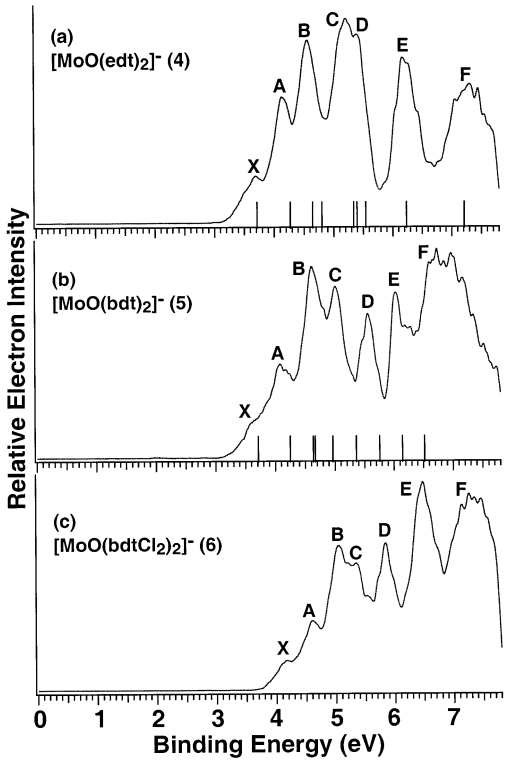


***Figure 4.*** Photoelectron spectra of (a) $[MoO(edt)_2]^-$ (**4**), (b) $[MoO(bdt)_2]^-$ (**5**), and (c) $[MoO(bdtCl_2)_2]^-$ (**6**) at 157 nm. The solid bars are the molecular orbital energy levels calculated using Koopmanns' approximation (see text and Tables 4 and 5).

etries were derived from the crystal structures of $(PPh_4)[MoO(edt)_2]$ and $(PPh_4)[MoO(bdt)_2]$,[69,70] respectively, with the coordinates adjusted such that the Mo−O bond is coincident with the *z*-axis and the average point of the four sulfur atoms is coincident with the *xz*-plane (see Supporting Information).[76] The calculations were performed in the spin-restricted mode. Scalar relativistic effects were included in the calculation using the zero-order regular approximation (ZORA).[76−79] All electron basis sets were used for all atom types except Mo, which was frozen to the 3d level. The relativistic potentials necessary for each atom were calculated using the auxiliary program DIRAC, which is supplied with the ADF program package. The density functional for all calculations used a generalized gradient approximation, with the exchange correction of Becke[80] and the correlation correction of Lee et al.[81]

## Results

**Monodentate Complexes.** Figure 3 shows the 157 nm PES spectra of the three monodentate complexes, **1**−**3**. The spectrum of **1** (Figure 3a) is relatively simple, revealing five well-resolved peaks (X, A−D). The lowest binding energy peak, X, with a vertical detachment energy (VDE) of 4.68 eV, is well separated from the higher binding energy features. The energy gap between X and A is as large as 1.32 eV. The intensities of the X and A features are weaker than those of the three higher binding energy peaks (B, C, D). The spectrum of **2** (Figure 3b) shows a well-resolved threshold peak (X) at a VDE of 3.46 eV. This peak is similar to the threshold peak of **1** (Figure 3a) in terms of both its shape and relative intensity. Following an energy gap of ∼0.79 eV, a broad band between 4.0 and 5.6 eV was revealed in the spectrum of **2**. The spectrum in this energy range is likely to contain numerous overlapping features, but three (A, B, C) were tentatively identified for later discussions. At even higher binding energies above 6 eV, more overlapping features were observed (D, E, F). The spectrum of **3** (Figure 3c) is very similar to that of **2**, except that it is shifted to higher binding energies by ∼0.4 eV due to the inductive effects of the Cl-substituted ligands. Again, a well-resolved threshold peak (X) was observed at a VDE of 3.89 eV, followed by an energy gap of ∼0.76 eV. We note that the energy gaps between X and A of **2** and **3** are nearly identical, but they are considerably smaller than that of **1**.

**Bidentate Complexes.** Figure 4 shows the 157 nm spectra of **4**−**6**, each with two dithiolate ligands. These spectra are similar to each other in overall spectral patterns but are quite different from those of **1**−**3**. Seven detachment features were resolved in each case, as labeled by the letters in Figure 4. A weak threshold feature (X) was again observed in all the spectra, similar to that observed in the spectra of **1**−**3**. But the gap between the X and A bands is considerably smaller in **4**−**6** than that in **1**−**3**. The spectra of **5** and **6** are almost identical in terms of spectral patterns, except that the spectrum of **6** was shifted to higher binding energies by ∼0.5 eV, again due to the

(73) Versluis, L.; Ziegler, T. *J. Chem. Phys.* **1988**, *88*, 322−329.
(74) te Velde, G.; Baerends, E. J. *J. Comput. Phys.* **1992**, *99*, 84−98.
(75) Fonseca Guerra, C.; Snijders, J. G.; te Velde, G.; Baerends, E. J. *Theor. Chem. Acc.* **1998**, *99*, 391−399.
(76) van Lenthe, E.; Baerends, E. J.; Snijders, J. G. *J. Chem. Phys.* **1994**, *101*, 9783−9789.
(77) van Lenthe, E.; Snijders, J. G.; Baerends, E. J. *J. Chem. Phys.* **1996**, *105*, 6505−6512.
(78) van Lenthe, E.; Leeuwen, R. v.; Baerends, E. J.; Snijders, J. G. *Int. J. Quantum Chem.* **1996**, *57*, 281−289.
(79) van Lenthe, E.; Ehlers, A. E.; Baerends, E. J. *J. Chem. Phys.* **1999**, *110*, 8943−8950.
(80) Becke, A. D. *Phys. Rev. A* **1988**, *38*, 3098−3100.
(81) Lee, C.; Yang, W.; Parr, R. G. *Phys. Rev. B* **1988**, *37*, 785−793.

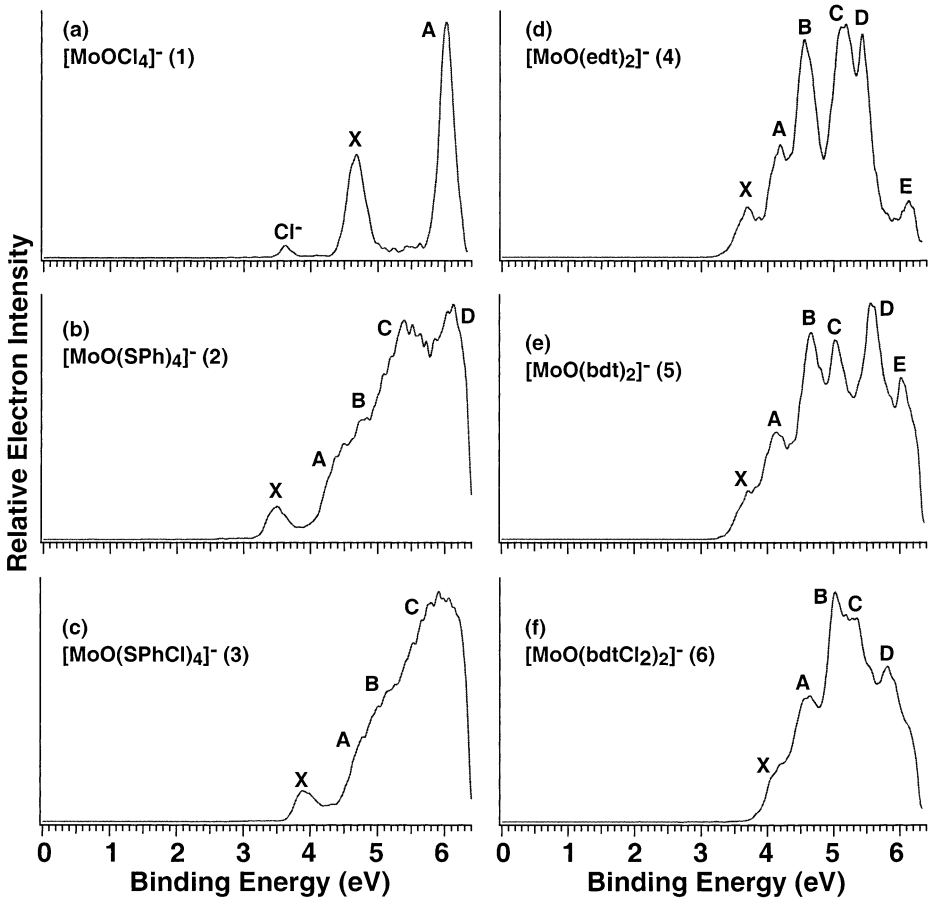


***Figure 5.*** Photoelectron spectra of $[MoOS_4]^-$ anions, **1**−**6**, at 193 nm (6.424 eV).

inductive effects of the Cl-substituted ligands in the latter. In addition, the relative intensity of feature E seemed to be enhanced in the spectrum of **6** (Figure 4c).

**PES Spectra at 193 and 266 nm.** We also obtained PES spectra at 193 nm for all six complexes (Figure 5) and at 266 nm for **2**, **3**, and **5** (not shown). The lower photon energy spectra were better resolved for the lower binding energy features. The 266 nm spectra are not shown because they did not reveal much new spectral information. However, the lower photon energy data yielded more accurate adiabatic detachment energies (ADEs) for the threshold feature. The very weak feature at 3.6 eV in the 193 nm spectrum of $[MoOCl_4]^-$ (Figure 5a) is from photodetachment of $Cl^-$, a fragmentation product from the parent complex. Overall, the 193 nm spectra revealed the same features as in the 157 nm spectra up to the 193 nm photon energy, with slightly better spectral resolution and some intensity variations.

**ADEs.** The ADEs of the threshold peak (X) represent the electron affinities of the neutral species in each case and are related to the redox properties of the metal complexes in solution. The ADEs were determined from the 193 nm spectra for **1**, **4**, and **6** and from the 266 nm spectra for **2**, **3**, and **5** because of the slightly better resolution of the X peak in the lower photon energy spectra. The VDE of each feature was measured straightforwardly from the peak maximum. Due to the lack of vibrational resolution, the ADE was measured by drawing a straight line along the leading edge of the X band and then adding a constant to the intersection with the binding energy axis to take into account the finite resolution and thermal broadening. Thus, the ADEs measured from the lower photon energy spectra were more accurate. The ADE and VDE of the X peak of **1**−**6** are listed in Table 1. The VDEs of all observed features are given in Tables 2−5.

***Table 1.*** Experimental Adiabatic (ADEs) and Vertical (VDEs) Detachment Energies for $[MoOCl_4]^-$ (**1**), $MoO(SPh)_4]^-$ (**2**), $[MoO(SPhCl)_4]^-$ (**3**), $[MoO(edt)_2]^-$ (**4**), $[MoO(bdt)_2]^-$ (**5**), and $[MoO(bdtCl_2)_2]^-$ (**6**) in eV

| | ADEs[a] | VDEs[a] | difference, VDE − ADE |
|---|---|---|---|
| **1** | 4.43(8) | 4.67(8) | 0.24 |
| **2** | 3.28(8) | 3.46(8) | 0.18 |
| **3** | 3.68(8) | 3.89(8) | 0.21 |
| **4** | 3.35(8) | 3.70(8) | 0.35 |
| **5** | 3.42(8) | 3.70(10) | 0.28 |
| **6** | 3.88(8) | 4.17(8) | 0.29 |

[a] The numbers in parentheses represent the uncertainty in the last digit.

## Discussion

**Overview of the Electronic Structures of $[MoOS_4]^-$.** The PES features shown in Figures 3−5 represent transitions from the ground state of the anions to the ground and excited states of the corresponding neutral molecules. Within the single-particle approximation (Koopmans' theorem), these PES features can be viewed as removing electrons from the occupied molecular orbitals (MOs) of the anions. Therefore, unlike other various experimental methods based on electronic transitions from occupied MOs to empty or partially empty MOs, PES directly maps out the energy levels of the occupied MOs. It

***Table 2.*** Experimental Vertical Detachment Energies (VDEs) and Calculated MO Levels in eV for $[MoOCl_4]^-$ (**1**), and the Assignments of the PES Spectra

| VDEs[a] | MO levels (**1**)[b] | assignment[c] |
|---|---|---|
| 4.68(8) (X) | 4.68 | $d_{xy}$ ($b_2$) |
| 6.00(8) (A) | 5.92 | Cl in-plane ($a_2$) |
| 6.76(8) (B) | 6.51 | Cl in-plane ($e$) |
| | 6.54 | Cl out-of-plane ($b_1$) |
| 7.08(8) (C) | 6.86 | Cl out-of-plane ($e$) |
| 7.23(8) (D) | 7.35 | Cl out-of-plane ($a_1$) |

[a] The numbers in parentheses represent the uncertainty in the last digit. [b] Taken from spin-unrestricted DFT calculations in idealized $C_{4v}$ crystal coordinates (from ref 82). The calculated MO levels were obtained by shifting the DFT $d_{xy}$ MO level to the VDE of the X feature. [c] The Cl in-plane and out-of-plane MOs are also referred to as Cl 3p($\pi$) and Cl 3p(pseudo-$\sigma$), respectively.

***Table 3.*** Experimental Vertical Detachment Energies (VDEs) and Calculated MO Levels in eV for $[MoO(SPh)_4]^-$ (**2**) and $[MoO(SPhCl)_4]^-$ (**3**), and the Assignments of Their PES Spectra

| VDEs (**2**)[a] | MO levels (**2**)[b] | assignment[c] | VDEs (**3**)[a] |
|---|---|---|---|
| 3.46(8) (X) | 3.46 | $(d_{xy})^{-1}$ | 3.89(8) (X) |
| 4.25(15) (A) | 4.67 | $[e(\pi)]^{-1}$ | 4.65(15) (A) |
| 4.70(15) (B) | 5.01 | $[a(\pi)]^{-1}$ | 5.10(15) (B) |
| 5.17(15) (C) | 5.12 | $[b(\pi)]^{-1}$ | 5.55(15) (C) |
| 6.25(10) (D) | 5.25 | $[e$(pseudo-$\sigma)]^{-1}$ | 6.90(20) (D) |
| 6.55(10) (E) | 6.02 | $[a$(pseudo-$\sigma)]^{-1}$ | 6.90(20) (E) |
| 7.00(15) (F) | 6.45 | $[b$(pseudo-$\sigma)]^{-1}$ | 7.45(10) (F) |

[a] The numbers in parentheses represent the uncertainty in the last digit. [b] Taken from the spin-restricted DFT calculated energies of the S 3p frontier MO levels for the model compound $[MoO(SCH_3)_4]^-$ at the same geometry as $[MoO(SPh)_4]^-$, but with the calculated energies shifted so that the HOMO $4d_{xy}$ MO level aligns with the VDE of the X peak in the PES spectrum. From ref 45. [c] The S 3p(pseudo-$\sigma$) MOs lie in the $xy$-plane and the S 3p($\pi$) MOs lie out of the $xy$-plane in the $C_4$ tetrathiolate complexes.

***Table 4.*** Experimental Vertical Detachment Energies (VDEs) and Calculated MO Levels[a] in eV for $[MoO(edt)_2]^-$ (**4**), and the Assignments of the PES Spectra

| VDEs (**4**)[b] | MO levels | assignment |
|---|---|---|
| 3.70(8) (X) | 3.70 | $(d_{x^2-y^2})^{-1}$ |
| 4.17(8) (A) | 4.26 | $[a_2(\pi)]^{-1}$ |
| 4.56(8) (B) | 4.64 | $[b_1(\pi)]^{-1}$ |
| | 4.80 | $[b_2(\pi)]^{-1}$ |
| 5.18(8) (C) | 5.32 | $[b_1$(pseudo-$\sigma)]^{-1}$ |
| 5.40(8) (D) | 5.40 | $[a_1(\pi)]^{-1}$ |
| | 5.54 | $[b_2$(pseudo-$\sigma)]^{-1}$ |
| 6.22(8) (E) | 6.25 | $[a_2$(pseudo-$\sigma)]^{-1}$ |
| 7.30(10) (F) | 7.21 | $[a_1$(pseudo-$\sigma)]^{-1}$ |

[a] Although the crystal coordinates employed reveal a low symmetry distortion from idealized $C_{2v}$ geometry, the $C_{2v}$ nomenclature is retained for describing the MOs derived from the spin-restricted DFT calculations. The normalization and alignment procedure for the calculated MO levels is discussed in the text. [b] The numbers in parentheses represent the uncertainty in the last digit.

should be pointed out, however, that Koopmans' theorem only provides a useful first approximation because it does not take into account relaxation effects, and the relationship of DFT Kohn−Sham orbital energies to ionization energies is not clearly defined beyond the highest occupied molecular orbital (HOMO). Nevertheless, it has been shown that a very good empirical correspondence exists between DFT Kohn−Sham orbital energies and the corresponding vertical ionization potentials determined by PES.[82] For anions involved in ET reactions, PES data yield the intrinsic oxidation energy of the free anions since photodetachment is an oxidation process.

(82) Chong, D. P.; Gritsenko, O. V.; Baerends, E. J. *J. Chem. Phys.* **2002**, *116*, 1760−1772.

***Table 5.*** Experimental Vertical Detachment Energies (VDEs) and Calculated MO Levels in eV for $[MoO(bdt)_2]^-$ (**5**) and $[MoO(bdtCl_2)_2]^-$ (**6**), and the Assignments of Their PES Spectra

| VDEs (**5**)[a] | MO levels[b,c] | assignment[c] | VDEs (**6**)[a] |
|---|---|---|---|
| 3.70(10) (X) | 3.70 | $(d_{x^2-y^2})^{-1}$ | 4.15(8) (X) |
| 4.12(8) (A) | 4.23 | $[a_2(\pi)]^{-1}$ | 4.61(8) (A) |
| 4.65(8) (B) | 4.64 | $[b_1(\pi)]^{-1}$ | 5.03(8) (B) |
| | 4.69 | $[b_2(\pi)]^{-1}$ | |
| 5.02(8) (C) | 4.96 | $[a_1(\pi)]^{-1}$ | 5.27(8) (C) |
| 5.58(8) (D) | 5.38 (5.40) | $[b_1$(pseudo-$\sigma)]^{-1}$ | 5.84(8) (D) |
| | 5.77 | $[b_2$(pseudo-$\sigma)]^{-1}$ | |
| 6.04(8) (E) | 6.16 (6.18) | $[a_1$(pseudo-$\sigma)]^{-1}$ | 6.48(8) (E) |
| | 6.51 | $[a_2$(pseudo-$\sigma)]^{-1}$ | |
| 6.85(15) (F) | | | 7.33(10) (F) |

[a] The numbers in parentheses represent the uncertainty in the last digit. [b] Values in parentheses are derived from normalizing the energies of the $S_{ip}\rightarrow$Mo $d_{x^2-y^2}$ CT transitions assigned to the two lowest electronic absorption bands of **5** (from ref 47). [c] Although the crystal coordinates employed reveal a low symmetry distortion from the idealized $C_{2v}$ structure of $[MoO(bdt)_2]^-$, the $C_{2v}$ nomenclature is retained to label the MO levels derived from the spin-restricted DFT calculations. The normalization and alignment procedure for the calculated MO levels is discussed in the text.

The electronic configuration for the metal in the $[Mo^VOS_4]^-$ centers is formally $4d^1$. It is widely accepted that the strong $\sigma$- and $\pi$-donor properties of the axial oxo ligand largely determine the electronic structure of the chromophore, destabilizing the $4d_{z^2}$ and $4d_{xz}/4d_{yz}$ orbitals within the d orbital manifold in the molecular frame (the axial Mo═O bond vector is defined as the $z$-axis).[66] This oxo-mediated destabilization in the presence of a moderate equatorial ligand field results in the unpaired electron residing in an MO of predominantly Mo $d_{xy}$ character in $C_{4v}$ symmetry (or $d_{x^2-y^2}$ in $C_{2v}$) to give a doublet ground state for $[MoOS_4]^-$. Beneath this d orbital manifold, there is a set of eight ligand-based symmetry-adapted linear combinations (SALCs) consisting of the lone pairs of the ligand S atoms. Four are primarily S 3p($\pi$) MOs, and four are primarily S 3p-(pseudo-$\sigma$) MOs. The energies of the S 3p($\pi$) MOs strongly depend on the O−Mo−S−C(α) dihedral angle, whereas the energies of the S 3p(pseudo-$\sigma$) MOs are relatively independent of this angle. For a $[MoOS_4]^-$ center with four monodentate thiolate ligands and idealized $C_{4v}$ symmetry, the S 3p($\pi$) MOs are optimally oriented for in-plane $\pi$-bonding with the Mo $4d_{xy}$ orbital (O−Mo−S−C(α) = 0°). At the observed equilibrium $C_4$ geometry with an O−Mo−S−C(α) dihedral angle of ∼59°, the primary $d_\pi-p_\pi$ interaction is decreased, and the S 3p($\pi$) MOs are generally at higher energies (less stabilized) than the S 3p(pseudo-$\sigma$) MOs. A synchronous rotation about the Mo−S bonds causes the S 3p($\pi$) orbitals to rotate out of the four-S plane, such that at the $C_4$ limit [O−Mo−S−C(α) = 90°] these S 3p($\pi$) orbitals are now oriented orthogonal to $d_{xy}$ and parallel to the Mo═O bond vector. A similar situation occurs for the bis-dithiolate compounds with idealized $C_{2v}$ symmetry, where the rigid geometry imposed on the S ligand donor atoms by the chelate ring constrains the S 3p($\pi$) orbitals such that they are oriented out of the $xy$-plane and orthogonal to the S 3p(pseudo-$\sigma$) MOs within the plane.[45] Such a Walsh diagram for the energies of the MOs of $[MoOS_4]^-$ has been derived from density functional calculations and used to interpret the electronic absorption and MCD spectra of the corresponding species.[45−47]

**Singlet−Triplet Splitting and the Observed PES Features for the $[MoOS_4]^-$ Complexes.** The ground states of the anions, **1**−**6**, are all open-shell with one unpaired 4d electron. Detaching this unpaired d electron gives rise to the closed-shell ground

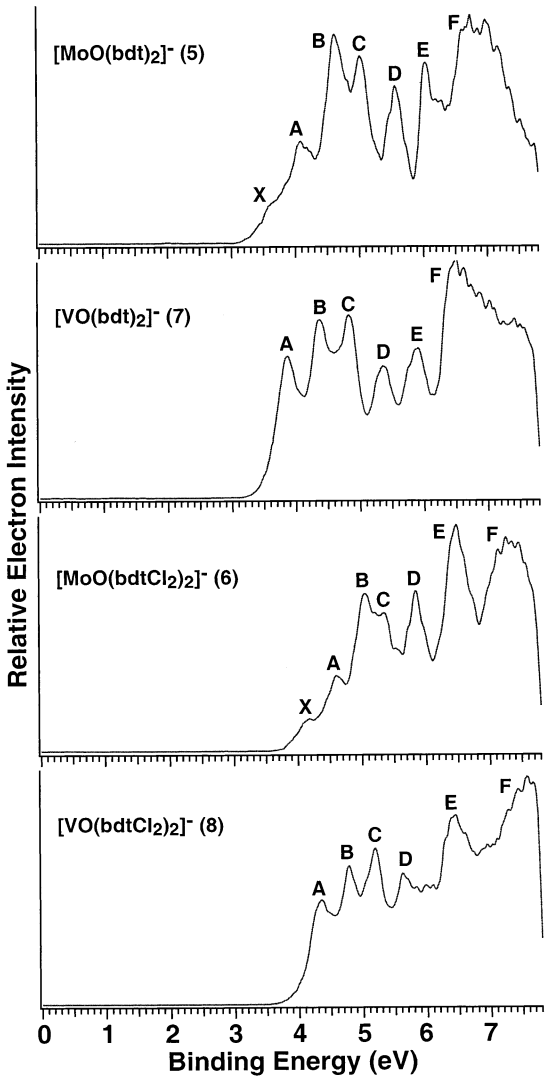


***Figure 6.*** Comparison of the 157 nm photoelectron spectra of $[MoOS_4]^-$ with those of $[VOS_4]^-$ complexes.

state of the neutral molecules, corresponding to the lowest binding energy feature (X) in each spectrum. Removal of one electron from the deeper MOs can result in two states (triplet or singlet), depending on the spin of the detached electron. Without knowing the triplet−singlet separation, it is difficult to assign the spectral features using the corresponding MO configurations of the anions.

To evaluate the triplet−singlet separation, we further obtained PES spectra of two analogous $[VOS_4]^-$ complexes, in which V is formally in the 5+ oxidation state with a $3d^0$ configuration. The PES features of these complexes correspond to transitions from the singlet ground state of the anions to the ground and excited states of the neutral molecules, which should all be doublet states. The 157 nm PES spectra of $[VO(bdt)_2]^-$ (**7**) and $[VO(bdtCl_2)]^-$ (**8**) are compared with those of the corresponding Mo complexes in Figure 6. Except for the lowest binding energy peak (X), the spectral features (A−F) of the Mo complexes (**5** and **6**) are very similar to those of the V complexes (**7** and **8**) and have a one-to-one correspondence, as labeled in Figure 6. The X features in the Mo complexes are due to removal of the single metal 4d electron, which is not present in the $3d^0$ V complexes. The similarity of the spectral features between the Mo and V complexes, in particular, the one-to-one correspondence for the features labeled A−F, suggests that either (1) the singlet−triplet splitting for the Mo complexes is too small to be resolved, (2) the splitting is very large and the singlet components are all outside our spectral range, or (3) the peaks for one of the spin states are very broad and weak and not resolved as spectral features. Since the PES features for **1**−**6** cover an energy range of ∼4.0 eV and the features in the spectra of **4**−**6** are reasonably well resolved, the scenarios of (2) and (3) seem unlikely. Thus, the triplet−singlet components derived from detachment from a completely filled MO in the Mo complexes would be contained in one single PES band. This results in the similarity observed between the spectral features of the analogous Mo and V complexes, despite their different ground-state electronic configurations. This interpretation is consistent with the spin-unrestricted calculations of McMaster et al.[45] for $[MoO(edt)_2]^-$, which showed that the energy levels of the SALCs in $\beta$-spin orbitals were all within 0.15 eV of the corresponding $\alpha$-spin orbitals. With this knowledge, as well as the previous optical spectroscopic data (electronic absorption and MCD),[2,45−47] we can tentatively assign all the PES features of the five $[MoOS_4]^-$ complexes.

***Table 6.*** Experimental Vertical Detachment Energies (VDEs) in eV for $[VO(bdt)_2]^-$ (**7**) and $[VO(bdtCl_2)_2]^-$ (**8**) Compared to Those for $[MoO(bdt)_2]^-$ (**5**) and $[MoO(bdtCl_2)_2]^-$ (**6**)[a]

| | $[MoO(bdt)_2]^-$ (**5**) | $[VO(bdt)_2]^-$ (**7**) | $[MoO(bdtCl_2)_2]^-$ (**6**) | $[VO(bdtCl_2)_2]^-$ (**8**) |
|---|---|---|---|---|
| X | 3.70(10) | | 4.15(8) | |
| A | 4.12(8) | 3.86(8) | 4.61(8) | 4.35(8) |
| B | 4.65(8) | 4.37(8) | 5.03(8) | 4.78(8) |
| C | 5.02(8) | 4.82(8) | 5.27(8) | 5.19(8) |
| D | 5.58(8) | 5.35(10) | 5.84(8) | 5.62(8) |
| E | 6.04(8) | 5.89(10) | 6.48(8) | 6.42(10) |
| F | 6.85(15) | 6.50(10) | 7.33(10) | ∼7.5 |

[a] The numbers in parentheses represent the uncertainty in the last digit.

The VDEs of the spectral features (A−F) for $[MoO(bdt)_2]^-$ are ∼0.2−0.3 eV higher than those of the corresponding peaks for $[VO(bdt)_2]^-$. A similar trend is observed for $[MoO(bdtCl_2)_2]^-$ versus $[VO(bdtCl_2)_2]^-$ (Figure 6, Table 6). Furthermore, the intensity of the A band in the V complexes is stronger than the corresponding feature in the Mo complexes. As discussed below, all S-based MOs give rise to relatively strong peaks compared to the peaks of MOs of mainly metal d character. The weakness of the A feature in the Mo complexes suggests that the corresponding MO in the Mo complexes has considerable metal d contributions. The increase in covalency in the Mo−S bonds indicates more charge donations from the dithiolate ligands to the metal center and hence reduces the overall negative charges on the ligands, leading to the increased VDEs of the PES features due to ionization of the ligand S orbitals in the Mo complexes.

**PES Spectra of $[MoOCl_4]^-$ (1).** The $[MoOCl_4]^-$ anion displays $C_{4v}$ symmetry with the unpaired electron in the $d_{xy}$ orbital ($b_2$). This simple halide model complex serves as a prototype for understanding the more complicated electronic structure of the molybdenum tetrathiolate centers.[83−85] Both DFT[83] and discrete variational $X\alpha$ calculations[85] predicted that the unpaired d electron is located in an MO of predominantly Mo $4d_{xy}$ character. Just below this singly occupied d orbital,

(83) Swann J.; Westmoreland, T. D. *Inorg. Chem.* **1997**, *36*, 5348−5357.
(84) Sabel, D. M.; Gewirth, A. A. *Inorg. Chem.* **1994**, *33*, 148−156.
(85) Deeth, R. J. *J. Chem. Soc., Dalton Trans.* **1991**, 1895−1900.

there are three in-plane (ip) Cl 3p MOs, $a_2$(ip) and $e$(ip), followed by four out-of-plane (op) Cl 3p MOs, $b_1$(op), $e$(op), and $a_1$(op).[66] Such an MO scheme was confirmed previously and used to interpret electronic absorption and MCD spectra of $[MoOCl_4]^-$.[66] The well-resolved PES features for $[MoOCl_4]^-$ make the analysis and assignment relatively straightforward. The X peak is due to removal of one electron from the $4d_{xy}$ orbital ($b_2$), resulting in a closed-shell singlet neutral $MoOCl_4$. The features A−D are due to detaching one electron from the Cl 3p lone pairs, $a_2$(ip), $e$(ip), $b_1$(op), $e$(op), and $a_1$(op), respectively, as shown in Table 2. This assignment is also consistent with the recent DFT calculation.[83] By shifting the $d_{xy}$ MO level to the VDE of the X feature and using Koopmans' approximation, the calculated relative orbital energies are in good agreement with the PES data, as shown in Table 2 and Figure 3a. In fact, the strong intensity and the discernible shoulder observed for the B feature are consistent with the assignment to two detachment channels from $e$(ip) and $b_1$(op).

**PES Spectra of $[MoO(SPh)_4]^-$ (2) and $[MoO(SPhCl)_4]^-$ (3).** The X-ray crystal structure of $[AsPh_4][MoO(SPh)_4]$ revealed a $[MoO]^{3+}$ unit coordinated by four S donors in a square pyramidal geometry of approximately $C_{4v}$ symmetry.[86] However, the average O−Mo−S−C(α) dihedral angle ($\theta$) is 58.8°, and this synchronous distortion from idealized $C_{4v}$ symmetry (where $\theta = 0°$ for $C_{4v}$) results in **2** possessing effective $C_4$ symmetry ($0° < \theta \leq 90°$ for $C_4$). Under $C_4$ symmetry, the frontier MOs predicted from recent DFT calculations[45] are $b(4d_{xy}) < e(\pi) < a(\pi) < b(\pi) < e$(pseudo-$\sigma$) < $a$(pseudo-$\sigma$) < $b$(pseudo-$\sigma$). The $b(4d_{xy})$ HOMO was predicted to be well separated from the $\pi$ and $\sigma$ MOs derived from the S lone pairs. This MO pattern is in excellent agreement with the observed PES spectra for **2** and **3** (Figure 3). Thus, the X feature is clearly due to detachment of the single d electron from the $b(4d_{xy})$ HOMO of **2** and **3**. The higher binding energy features in the spectra of **2** and **3** appeared to group in two broad energy ranges, labeled as A−C and D−F. These features should be due to detachments from the $\pi$ and $\sigma$ MOs of the S lone pairs. The energy gaps between X and A are nearly the same in **2** and **3** (∼0.8 eV) but are much smaller than the energy gap between X and A in $[MoOCl_4]^-$ (1.32 eV), due to the lower ionization potentials of the S lone pairs of the thiolate ligand compared to the ionization potentials of the $Cl^-$ ligands. The vertical lines in Figure 3b represent the calculated energies of the S 3p frontier MO levels for the model compound $[MoO(SCH_3)_4]^-$ at the same geometry as $[MoO(SPh)_4]^-$ (**2**),[45] but with the calculated energies shifted such that the HOMO $4d_{xy}$ level aligns with the VDE of the X peak in the PES spectrum (Table 3). The calculated MO energy levels of the S 3p lone pairs are grouped as $e(\pi)-a(\pi)-b(\pi)-e$(pseudo-$\sigma$) and $a$(pseudo-$\sigma$)−$b$(pseudo-$\sigma$). Although detailed assignments are not feasible due to the congested nature of the high binding energy features, the calculated MO energies for the S lone pairs are in excellent qualitative accord with the observed PES patterns for both **2** and **3**.

**PES Spectra of $[MoO(edt)_2]^-$ (4), $[MoO(bdt)_2]^-$ (5), and $[MoO(bdtCl_2)_2]^-$ (6).** The PES spectra of **4**−**6** are similar to each other (Figure 4), except that the C and D bands appeared to be more closely spaced in the spectrum of **4** than in the spectra of **5** and **6**. The overall spectral similarity between **4** and **5** strongly suggests that the observed PES features have similar electronic origins. However, the spectra of the three bidentate Mo complexes are qualitatively different from those of the monodentate complexes (**2** and **3**). The PES data clearly show that the rigid C−C backbones of the edt, bdt, and $bdtCl_2$ chelating ligands have a significant effect on the electronic structure and chemical bonding of the Mo complexes. First, the X−A energy gap is much smaller for the three dithiolate complexes, ∼0.47 eV for **4**, ∼0.42 eV for **5**, and ∼0.46 eV for **6**, compared to ∼0.8 eV for **2** and **3**. The reduced X−A gaps result in partial overlap of the two PES features (Figure 4). Second, in contrast to **2** and **3**, where the PES features (A−F) are grouped in two binding energy ranges and are rather congested, the A−F features of **4**−**6** are more equally spaced in a similar overall binding energy range and are much better resolved.

It has been predicted that the O−Mo−S−C dihedral angle plays an important role in determining the orientation of the S lone pairs, with respect to the Mo 4d orbitals, and the energy separations.[45] The structures of the molybdenum dithiolate complexes possess effective $C_{2v}$ symmetry, and the O−Mo−S−C dihedral angles are constrained (i.e., $\theta = \sim 90°$), whereas the dihedral angle is ∼59° for complexes **2** and **3** ($C_4$). With the 90° dihedral angle, the energy separation between the occupied 4d orbital and the highest occupied S-based MO is predicted to be substantially less than the analogous separation in $[MoO(SPh)_4]^-$. Our observed PES patterns for **2**−**6** are in remarkable agreement with the Walsh diagram derived from the previous DFT calculations,[45] depicting the changes of the frontier MOs of a model $[MoOS_4]^-$ complex, $[MoO(SMe)_4]^-$, as a function of the O−Mo−S−C dihedral angle. The Walsh diagram (Figure 6 in ref 45) predicts that, at an O−Mo−S−C dihedral angle of 58.8°, appropriate for **2** and **3**, there is a reasonably large gap between the 4d HOMO and the top of the S-based MOs, which are congested into two groups. On the other hand, at a dihedral angle of 90°, appropriate for **4**−**6**, the Walsh diagram predicts that the energy of the 4d HOMO is close to the top of the S-based MOs, which are now more evenly spaced, with the exception of the $a(\pi)$ and $e$(pseudo-$\sigma$) MOs in the middle of the diagram that are nearly degenerate. The two closely spaced PES features C and D in **4** are in excellent agreement with this latter prediction.

**Computational Studies and Further Considerations of the PES Data for $[MoO(edt)_2]^-$ (4) and $[MoO(bdt)_2]^-$ (5).** The DFT calculations on $[MoO(edt)_2]^-$ using both spin-restricted and spin-unrestricted methods showed that the Mo 4d manifold and some of the S 3p($\pi$)-based MOs were very close in energy for idealized $C_{2v}$ symmetry.[45] For the spin-unrestricted DFT calculations on $[MoO(edt)_2]^-$, the similar energies of the Mo 4d and S 3p($\pi$) orbitals produce a spin polarization between the occupied (α-spin) and unoccupied ($\beta$-spin) components of the $4d_{x^2-y^2}$ orbital, such that the α-spin $d_{x^2-y^2}$ MO lies lower in energy than the highest occupied S 3p($\pi$) MOs. However, the calculated energy of the unoccupied $\beta$-spin $d_{x^2-y^2}$ MO is within ∼0.1 eV of the highest occupied S 3p($\pi$) MOs. Since the $\beta$-spin $d_{x^2-y^2}$ MO is the lowest unoccupied molecular orbital that is metal-based, the results of these spin-unrestricted calculations were important for assigning the low-energy CT transitions to the $d_{x^2-y^2}$ redox acceptor orbital in the optical spectra of these compounds. Although these calculations (employing the highest

(86) Bradbury, J. R.; Mackay, M. F.; Wedd, A. G. *Aust. J. Chem.* **1978**, *31*, 2423−2430.

effective symmetry possible) provided a useful basis for interpreting the observed MCD transitions in $[MoO(edt)_2]^-$,[45] the previous computational results appear to be inconsistent with the current experimental observations, which indicate a singly occupied metal-based (4d) HOMO for **4**. A similar MO ordering was observed for **5** in the present DFT study using geometry-optimized $C_{2v}$ coordinates in spin-restricted and -unrestricted calculations (not discussed here). These discrepancies between the DFT calculations and the experimental PES data suggest that additional geometric and/or electronic effects must be considered in assigning the anionic PES features of **4** and **5**.

The actual symmetry of the $[MoO(edt)_2]^-$ anion in the solid state is approximately $C_2$,[69] lower than the idealized $C_{2v}$ symmetry employed in the previous calculations. This distortion in the crystal is evident from the twisting of the two $MoS_2$ chelate planes relative to each other. Therefore, we carried out further DFT calculations on $[MoO(edt)_2]^-$, using the geometric coordinates found in the crystal structure (Table S1, Supporting Information). These spin-restricted calculations correlate with those of McMaster et al.,[45] except that the $4d_{x^2-y^2}$ orbital becomes the HOMO in the current study. Beneath the d orbital manifold, there is a set of eight ligand-based SALCs that are primarily S 3p in character. The ordering of these orbitals is the same as that found by McMaster et al. (Table S2, Supporting Information).[45] The distortion away from $C_{2v}$ symmetry is due to the fact that the ligand carbon atoms have approximate tetrahedral geometry and the hydrogen atoms conform to a staggered rather than eclipsed configuration. The anion PES data imply that the distortion persists in the gas phase. The computational results enable the assignment of the PES spectral features of $[MoO(edt)_2]^-$ (**4**). The computational results are normalized to the PES features by shifting the $d_{x^2-y^2}$ MO level to the VDE of the X feature. The normalization procedure for the $[MoO(dithiolate)_2]^-$ complexes is the same used previously for the $[MoOCl_4]^-$ and $[MoO(SR)_4]^-$ compounds. The energy levels of the valence MOs can be aligned with the features A−E by adding the difference between the eigenvalues of the valence MOs and the HOMO to the VDE of the X feature in the spirit of Koopmans' approximation. The obtained relative orbital energies are in good agreement with the PES data, as shown in Table 4.

The X-ray crystal structure of $(PPh_4)[MoO(bdt)_2]$ shows that the anion in this crystal is also distorted from idealized $C_{2v}$ symmetry, as evidenced by the nonplanarity of one of the chelate rings.[70] The same effect, where one of the chelate rings is essentially planar and the other ring is folded along the S- - -S vector, forming a dihedral angle of 144° with the $MoS_2$ plane, is observed in the crystal structure of $(NEt_4)[MoO(cis\text{-ethylene-1,2-dithiolate})_2]$.[42] The similar structures of these two different $[MoO(ene\text{-}1,2\text{-}dithiolate)_2]^-$ anions in the $PPh_4^+$ salt[70] and the $NEt_4^+$ salt[42] suggest that the common distortion of these anions may be electronic in origin. We also performed DFT calculations, employing the crystal coordinates of $[MoO(bdt)_2]^-$ (Table S3, Supporting Information), to provide further insight into the PES features of **5** (geometry optimization calculations starting from these coordinates did not reach convergence). The results of the spin-restricted calculations for **5** correlate with the calculations of McMaster et al.[45] for the anion $[MoO(edt)_2]^-$, except that the $d_{x^2-y^2}$ orbital is calculated as being the HOMO. Again, beneath the d orbital manifold there is a set of eight ligand-based SALCs that are primarily S 3p in character. The four highest energy ones are primarily S 3p($\pi$) MOs, and the next four are primarily S 3p(pseudo-$\sigma$) MOs. This calculated ordering of the MOs corresponds with the anion PES spectra of **5** and **6**, which show that the HOMO is metal-based. The HOMO of $[MoO(bdt)_2]^-$ (Figure 7), obtained from calculations using the crystal structure coordinates, reveals the effect of the distortion from idealized $C_{2v}$ symmetry induced by the nonplanarity (folding) of one of the chelate rings. The results show that a considerable amount of S 3p character (21%) is present in the $d_{x^2-y^2}$ redox orbital, suggesting that indeed this folding is electronic in origin. Specifically, the electronic structure calculations reveal that the symmetry reduction in **5** (and in **4)** results in a substantial increase in the dithiolate sulfur (3p) character mixed into the HOMO. The DFT results obtained using the crystallographic coordinates show that the HOMO in both **5** and **4** is primarily metal based (Mo 4d) and is more covalent due to the additional Mo 4d−S $3p_\pi$ mixing in the lower symmetry. The covalency in the metal-based HOMO of **5** (52.6% $d_{x^2-y^2}$) is similar to that in each of the structures calculated for **2** (53% $4d_{xy}$) and **4** (55.4% $d_{x^2-y^2}$), as illustrated by the amount of Mo 4d character. Table S4 (Supporting Information) gives the relative energies of the MOs and their atomic composition for **5**. The compound has pseudo-$C_{2v}$ symmetry, and symmetry labels for this point group are included for convenience. These computational results again enable a qualitative assignment of the PES spectral features of **5**, implying that the distortion away from $C_{2v}$ symmetry persists for **5** in the gas phase. The shift procedure for normalizing and aligning the results of the molecular orbital calculations to the PES features was applied to **5** in a manner similar to that described above for **1**, **2**, and **4**. The calculated relative orbital energies are in good agreement with the PES data, as given in Table 5.

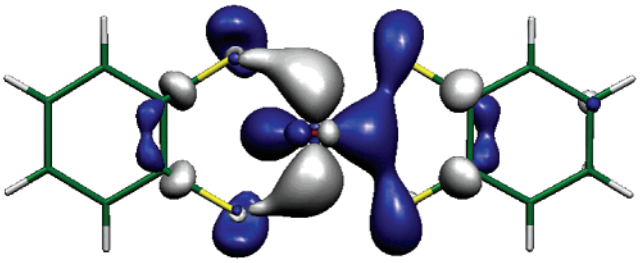

***Figure 7.*** MO contour of the HOMO in $[MoO(bdt)_2]^-$ derived from calculations using the crystal structure coordinates. The view is oriented such that the *z*-axis is directed along the Mo═O bond vector and projected out of the plane of the page.

The above assignments of the PES spectra of **4**−**6** imply that the lowest binding energy peaks (X) (Figure 4) are due to detachment of the unpaired d electron in each anion. This assignment is further supported by comparison between the PES spectra of $[MoO(bdt)_2]^-$ and $[VO(bdt)_2]^-$, as shown in Figure 6. The absence of a similar weak, low binding energy peak (X) in the formally $3d^0$ V complexes is expected. The calculations also support the argument that the MO of peak A has more metal character than the MOs of B−F, as suggested from their respective PES intensities in **4** and **5**. The MO ordering in **4** and **5** has been re-evaluated by the DFT calculations in light of the current experimental observations, which indicate that the HOMO of these complexes is due to the Mo 4d orbital. The

nature of the HOMO is important for understanding the reactivity of these complexes, in particular their redox properties.

**The ADEs and Redox Potentials.** A one-electron oxidation reaction, aside from solvation effects, is similar to electron detachment in the gas phase. Therefore, the gas-phase ADEs should be inherently related to oxidation potentials, except that the solvation effects are absent in the electron detachment in a vacuum. The X feature in the PES spectra of **1**−**6** (Figures 3−5) corresponds to removing the unpaired 4d electron from the HOMO of each species. The ADEs of **3** (3.68 eV) and **6** (3.88 eV) with Cl substituents on the thiolate ligands are ∼0.4 eV higher than those of **2** (3.28 eV) and **5** (3.42 eV), respectively, consistent with the electron-withdrawing effect of the Cl substituents. Similar inductive effects have also been observed in bulk redox potentials of related metal complexes.[68,87,88]

As we have shown previously,[62] the energy difference between the VDE and ADE of the X feature directly reflects the geometry changes after one electron is removed and, hence, is related to the intrinsic reorganization energy of an ET reaction. Among the five $[MoOS_4]^-$ complexes investigated here, the differences between VDE and ADE for the bis-dithiolate complexes are greater than those for the monodentate tetrathiolate anions (Table 1), implying larger geometry changes upon detaching the unpaired Mo 4d electrons for the bis-dithiolate complexes. This observation is consistent with the covalency differences between the constrained chelate versus the nonchelated systems. Although the DFT calculations presented here suggest similar sulfur contributions to the covalency of the HOMO, previous electronic absorption data support more Mo−S covalency for the HOMO in **2** relative to that for the HOMO in **4**.[45−47] The greater covalency of the HOMO in **2** relative to that of the HOMOs in **4** and **5** is implied by the greater CT intensity of the low-energy S→Mo $d_{xy}$ absorption bands in the nonchelated complexes compared to that of the corresponding transitions in the chelated complexes.[45−47] Further understanding of the nature and extent of the structural distortions that accompany ionization, and the relationship between reorganization energies and covalency differences in this series of $[MoOS_4]^-$ anions, will require detailed calculations on both the anions and the neutral species with full geometry optimization. Such detailed calculations are beyond the scope of this paper.

(87) Mader, M. L.; Carducci, M. D.; Enemark, J. H. *Inorg. Chem.* **2000**, *39*, 525−531.
(88) Inscore, F. E.; Joshi, H. K.; McElhaney, A. E.; Enemark, J. H. *Inorg. Chim. Acta* **2002**, *331*, 246−256.

## Conclusions

The electronic structures and chemical bonding of tetrathiolate $[Mo^VOS_4]^-$ centers with both monodentate and bidentate ligands were investigated by photodetachment photoelectron spectroscopy. The well-resolved lowest binding energy feature observed in the PES spectra is assigned to derive from an MO primarily of Mo $4d^1$ character, providing conclusive evidence that the HOMOs and the redox orbitals in these $[Mo^VOS_4]^-$ centers are all metal-based. The PES data further revealed that the energy gaps between the HOMO d orbital and the highest occupied S-based ligand orbitals are dependent on the O−Mo−S−C dihedral angles, which are influenced by bidentate versus monodentate ligation. The energy separations are relatively large for the complexes containing monothiolate ligands in which the dihedral angle is ∼59°, but much smaller for those possessing dithiolate ligands with a dihedral angle of ∼90°, consistent with previous theoretical predictions.[45−47] The higher energy PES features are due to removal of electrons from the ligand-based molecular orbitals that are primarily localized on sulfurs and can be assigned satisfactorily on the basis of comparison with previous and current theoretical calculations and MCD and electronic absorption data. The reorganization energies after removal of one electron from the redox orbital were observed to be larger for the bis-dithiolate complexes than for the tetramonothiolate compounds.

**Acknowledgment.** The authors thank Dr. Jon McMaster at Nottingham University for helpful discussions. Support by the National Institutes of Health (GM-37773 to J.H.E. and GM-63555 to L.S.W.) is gratefully acknowledged. The experimental work done in Washington was performed at the W.R. Wiley Environmental Molecular Sciences Laboratory, a national scientific user facility sponsored by the U.S. Department of Energy's Office of Biological and Environmental Research and located at Pacific Northwest National Laboratory, which is operated for the DOE by Battelle.

**Supporting Information Available:** Tables S1−S4, listing the atomic coordinates used in the density functional calculations and the results of the restricted DFT calculations for the frontier orbitals of $[MoO(edt)_2]^-$ (**4**) and $[MoO(bdt)_2]^-$ (**5**) (PDF). This material is available free of charge via the Internet at http://pubs.acs.org.

JA0265557